Supporting Information

Thermochromism of rapid response to temperature change *versus* mechanochromism in a Ni-dithiolene complex salt

Lei Xu,[a] Yi-Ming Wang,[a] Zi-Heng Feng,[a] Yin Qian,*[a] Yan Gao,[a] Zheng-Fang Tian,[b] Xiao-Ming Ren*[a,c]

[a] State Key Laboratory of Materials-Oriented Chemical Engineering and College of Chemistry and Molecular Engineering, Nanjing Tech University, Nanjing 211816, P. R. China

[b] Hubei Key Laboratory of Processing and Application of Catalytic materials, Huanggang Normal University, Huanggang, 438000, P.R. China

[c] State Key Laboratory of Coordination Chemistry, Nanjing University 210023, P. R. China

Email: yinqian@njtech.edu.cn (YQ); xmren@njtech.edu.cn (XMR)

Contents

comparison for sample-1 and sample-2, indicating that the temperature of phase transition is not affected by the flowing rate of N_2 gas.

Fig. S12: Variable-temperature PXRD patterns of **1** measured at 298 K for the sample (a) before heated (i.e., the as-synthesized sample) and after heated from 298→323→343→353→363→353→323→298 K, (b) the sample measured at 298 and 353 K together with the simulated pattern using the single crystal structure data at 303 K (inset Table showing the 2θ angles and Miller index of diffractions indicated as well as the packing diagram viewed along *a*-axis). (c) PXRD patterns of **1**, in which the black, red and blue plots represent the patterns of pristine, annealed at 363 K and then cooled down to room tempertaure, and simulated pattern from single crystal structure. The PXRD patterns of pristine sample and the one annealed at 363 K then cooled down to room temperature are almost the same, indicating that the structural phase transition is reversible.

Fig. S13: Photos of microcrystalline sample of $[C_8$-4,4'-BiPy][Ni(mnt)$_2$] at (a) 303 and (b) 353 K.

Fig. S14: (a) Solid UV-vis-near-IR spectra at different temperatures, where the black and blue plots represent the spectra of pristine sample at 298 K, 373 K, and the red curve is obtained that the sample was heated to 373 K and then cooled down to 298 K. Photos of microcrystalline sample of **1** at (b) 303 and (c) 353 K.

Fig. S15: Variable-temperature IR spectra of **1** in different spectral regions of (a) 4000–400 cm^{-1}, (b) 3150–2800 cm^{-1}, (c) 1650–1400 cm^{-1}, (d) 1200–900 cm^{-1}.

Fig. S16: DSC plots of ground for (a) 3 min, and (b) 5 min, which show one coupling of thermal anomaly with almost the same peak temperatures with the pristine sample of **1**.

Fig. S17: Temperature dependence of dielectric permittivity of **1** at selected AC frequencies in 180–478 K on cooling.

Table S3: Dielectric constants of some conventional high-κ metal-oxides

References

Experimental section

Materials

All reagents and chemicals were purchased from commercial sources and used directly. Disodium maleonitriledithiolate (Na_2mnt),[1] 1,1'-diheptyl-4,4'-bipyridinium dibromide ($[C_7$-4, 4'-BiPy$]Br_2$)[2] were prepared following the published procedures.

Synthesis of $[C_7$-4, 4'-BiPy$][Ni(mnt)_2]$ (1)

$[C_7$-4,4'-Bipy$][Ni(mnt)_2]$ (**1**): Na_2mnt (372 mg, 2 mmol) and $NiCl_2{\cdot}6H_2O$ (237 mg, 1 mmol) were mixed under stirring with 100 mL H_2O at ambient temperature, subsequently, a solution of $[C_7$-4, 4'-BiPy$]Br_2$ (486 mg, 1 mmol) with 30 mL H_2O was added to the mixture. The precipitate was immediately formed, and the mixed solution was vigorously stirred for 10 min. and then filtered off, washed with 15 mL of H_2O (3×5 mL). The crude product was transferred to a beaker with 15 mL of MeOH, and the mixture was further ultrasonicated for 10 min. to give light green microcrystals, which were collected by suction, with yield of ~88% (calc. based on $NiCl_2{\cdot}6H_2O$). Anal. Calc. for $C_{32}H_{38}N_6S_4Ni$ (**1**): C, 55.41; H, 5.52; N, 12.12%. Found: C, 55.31; H, 5.35; N, 12.14%.

The single crystals suitable for X-ray structure analysis were grown by diffusion method in a sealed test tube, i.e., the solution of **1** in 3 mL of DMF and 10 mL EtOH are placed on the bottom and top of a test tube, respectively. This tube was sealed at ambient temperature, and the plate-shaped crystals of **1** were obtained for ~10 days.

Physical measurements

Elemental analyses for C, H, and N were performed on an Elementar Vario EL III analytic instrument. IR spectra in 4000–400 cm^{-1} were recorded on a Bruker Vector 22 Fourier transform infrared spectrometer (170SX) using KBr pellet at ambient temperature. Temperature-dependent IR spectroscopy was performed in a Bruker Tensor FTIR instrument that was equipped with an attenuated total reflection cell (Harrick) (ATR-FTIR). Powder X-ray diffraction (PXRD) data were collected on a MiniFlex600 X-ray diffractometer with Cu Kα (λ = 1.5404 Å) radiation at ambient temperature. Temperature-dependent PXRD patterns were recorded by Bruker D8 ADVANCE instrument equipped with an xrk900 sample cell. Thermogravimetric (TG)

analyzer experiments were performed using a simultaneous SDT 2960 thermal, the sample was held in a platinum pan under nitrogen flow in the rate of 100 mL min^{-1} and heated at a ramping rate of 20 °C min^{-1} from 303 to 1073 K (from 30 to 800 °C). Differential scanning calorimeter (DSC) experiments were carried out on Shimadzu DSC-60 differential scanning calorimeter in the temperature range of 186–573 K (from −87 to 300 °C). Dielectric constant and loss measurements were carried out using Concept 80 system (Novo control, Germany) in the ranges of 1–10^7 Hz and 173–403 K; the powdered sample of **1** was pressed to a pellet with a thickness of ca. 1.09 mm and a diameter of 7.0 mm (an area of 38.5 mm^2) under a static pressure of 8 MPa for 5 min., which two surfaces were gold-plated, such pellet was sandwiched by the copper electrodes for dielectric measurements, and the temperatures range from 173 to 473 K and the alternating current (AC) frequencies change from 1 to 10^7 Hz. Variable-temperature solid-state UV-vis-NIR absorption spectra were recorded on a Shimadzu UV3600PLUS equipped with Integrating Spheres.

X-Ray single crystallography

Single-crystal X-ray diffraction data were collected on a Bruker D8 QUEST Apex III CCD area detector diffractometer with graphite-monochromated Mo Kα radiation (λ = 0.71073 Å) at room temperature. Data reduction and absorption correction were performed with the SAINT[3] and SADABS[4] software packages, respectively. The crystal structure was solved by direct method and refined on F^2 using full matrix least-squares method with SHELXTL package.[5] All hydrogen atoms were placed at the calculated positions and refined as riding on their parent atoms with fixed isotropic displacement parameters. X-ray diffraction data collection, structure refinement, and crystallography are summarized in Table S1.

Pawley refinement of PXRD pattern in in high-temperature phase

The tentative Pawley refinement of the diffraction pattern was performed for the diffraction data of **1** in HTP at 353 K using the Reflex module in Materials Studio. During the refinement of PXRD pattern in HTP, the crystal structure in LTP was used as the starting model structure and the background was removed.

Table S1: Crystal data and structure refinement parameters for **1**

Single crystal structure refinement		Pawley refinement
Chemical formula	$C_{32}H_{38}N_6NiS_4$	$C_{32}H_{38}N_6NiS_4$
CCDC number	2236097	
Formula weight	693.63	693.63
Temperature (K)	303(2)	353 K
Wavelength (Å)	0.71073	1.5418
Crystal system	Triclinic	Triclinic
Space group	*P*–1	*P*–1
a (Å)	7.3761(7)	7.341
b (Å)	8.4798(7)	8.509
c (Å)	14.8502(14)	17.734
α (°)	91.382(3)	91.03
β (°)	92.267(3)	91.58
γ (°)	107.566(3)	107.13
V (Å^3) / Z	884.21(14)/1	
D_{calc} (g/cm^3)	1.303	
Abs. coefficient (mm^{-1})	0.815	
F(000)	364	
θ range for data collection	1.373–27.657	
Index range	$-8 \le h \le 8$	
	$-10 \le k \le 10$	
	$-17 \le l \le 17$	
Reflections collected	11624	
Independent reflections	3186	
R_{int}	0.0665	
Refinement on F^2	Full-matrix least-squares	
Data / restraints / parameters	3186/7/196	
Goodness-of-fit on F^2	1.022	
Final *R* indices [$I > 2\sigma(I)$]	0.0593	
R indices (all data)	0.1155	
Residual (eÅ^{-3})	0.539/–0.393	

Table S2: Bond lengths (Å) and bond angles (°) in anion of **1**

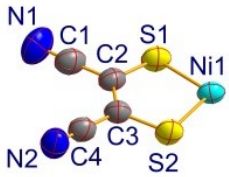

Bond length / Å		Bond angle / °	
Ni1–S1	2.1679(10)	S2–Ni1–S1	91.89(4)
Ni1–S2	2.1638(10)	C2–S1–Ni1	103.59(13)
S1–C2	1.724(4)	C3–S2–Ni1	103.48(14)
S2–C3	1.733(4)	N1–C1–C2	177.5(5)
N1–C1	1.141(6)	C3–C2–C1	122.2(4)
N2–C4	1.136(5)	C3–C2–S1	120.5(3)
C1–C2	1.433(6)	C1–C2–S1	117.3(3)
C2–C3	1.363(5)	C2–C3–C4	122.2(4)
C3–C4	1.428(6)	C2–C3–S2	120.3(3)
		C4–C3–S2	117.5(3)
		N2–C4–C3	177.7(4)

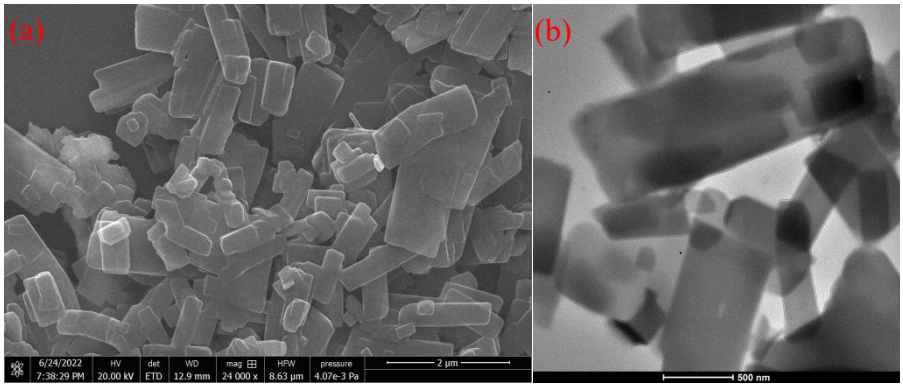

Fig. S1: Photos of (a) SEM and TEM for **1**.

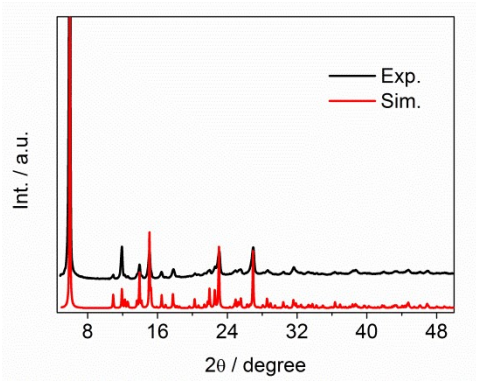

Fig. S2: Experimental and simulated PXRD patterns of **1**.

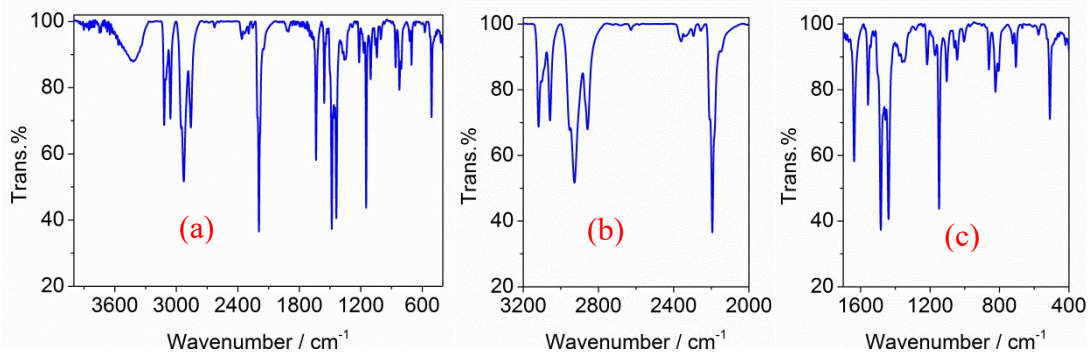

Fig. S3: IR spectrum of **1** in different spectral regions (a) 4000–400[1], (b) 3200–2000, (c) 1700–400 cm^{-1}.

Typical IR spectrum bands with assignments: Bands located at 3118.7s, 3101.4sh, 3087.9sh and 3057.0S are assigned to ν_{C-H} on the pyridyl rings. Bands with peaks at 2952.9sh, 2927.8s and 2858.4s arise from ν_{C-H} of CH_2 and CH_3 in heptyl groups. Bands centered at 2208.4sh, 2194.9s and 2183.2sh are assigned to $\nu_{C\equiv N}$. Bands located at 1483.2s and 862.1s arose from $\nu_{C=C}$ of mnt^{2-} and ν_{C-S}, respectively. The most intense vibrational band of $\nu_{C\equiv N}$ (less than 2200 cm^{-1}) together with the typical $\nu_{C=C}$ of mnt^{2-} and ν_{C-S} bands indicate that the valence of anion species is –2.[6]

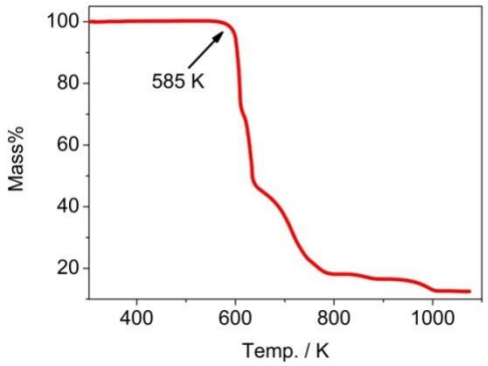

Fig. S4: TG plot of **1** in 303–1073 K.

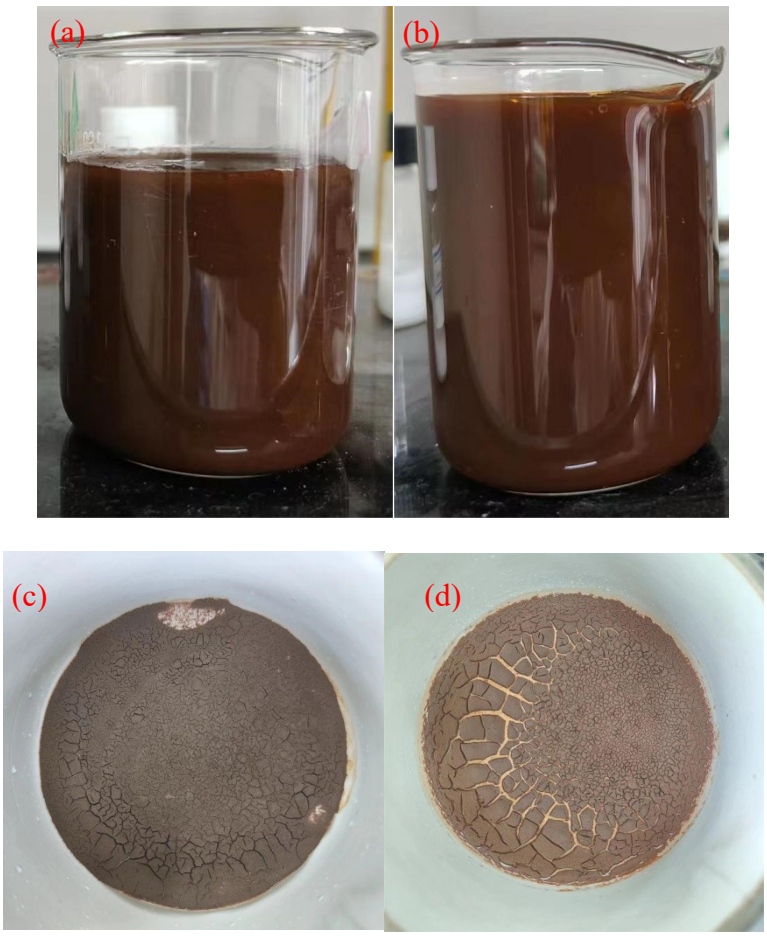

Fig. S5: Photos of (a) [C_8-4,4'-BiPy][Ni(mnt)$_2$] and (b) **1** precipitate immediately formed in aqueous solution. Photos of dried solids separated from aqueous solution of (c) [C_8-4,4'-BiPy][Ni(mnt)$_2$] and (d) **1**.

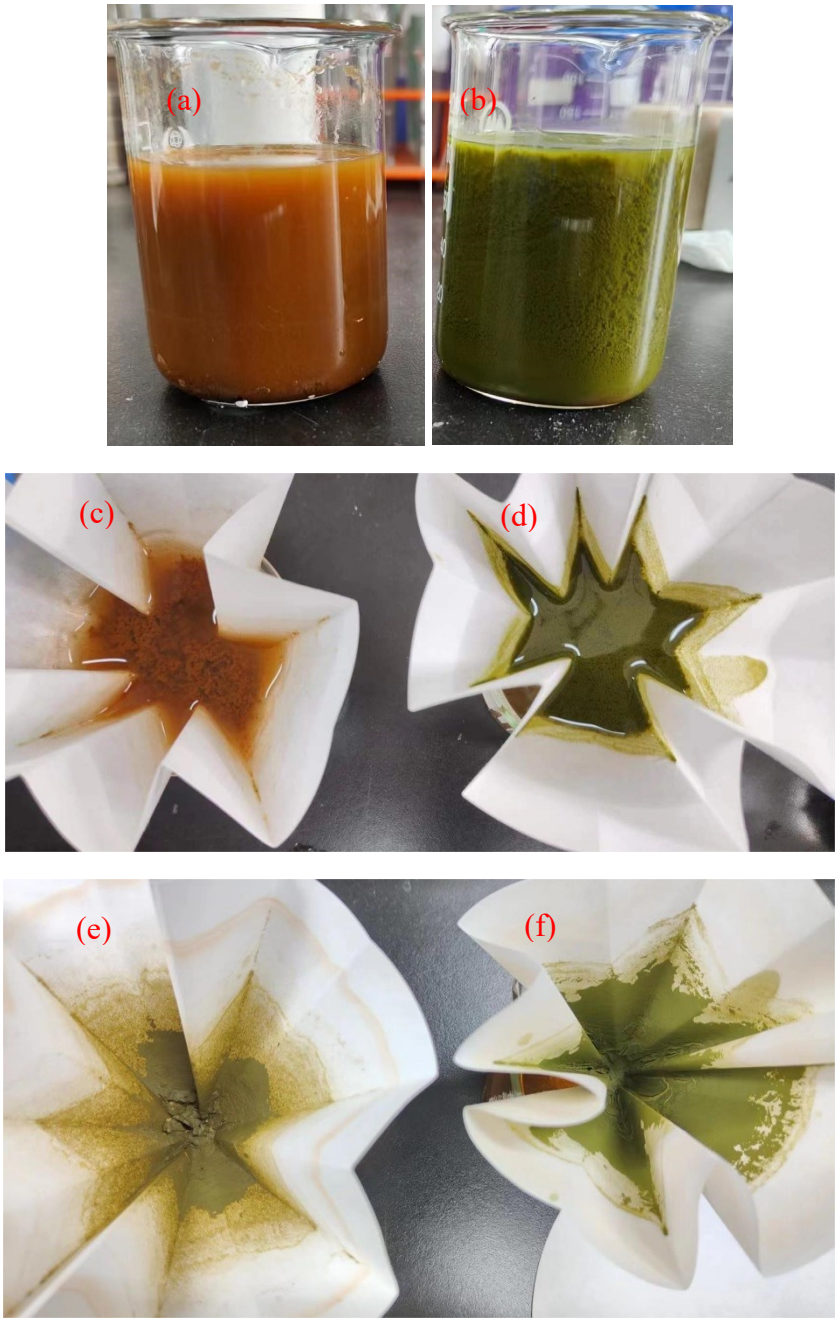

Fig. S6: Photos of (a) dried solids [C_8-4,4'-BiPy][Ni(mnt)$_2$] and (b) **1** dispersed in MeOH. Before filtrated from MeOH of (c) [C_8-4,4'-BiPy][Ni(mnt)$_2$] and (d) **1**. Dried solids after filtrated from MeOH of (e) [C_8-4,4'-BiPy][Ni(mnt)$_2$] and (f) **1**.

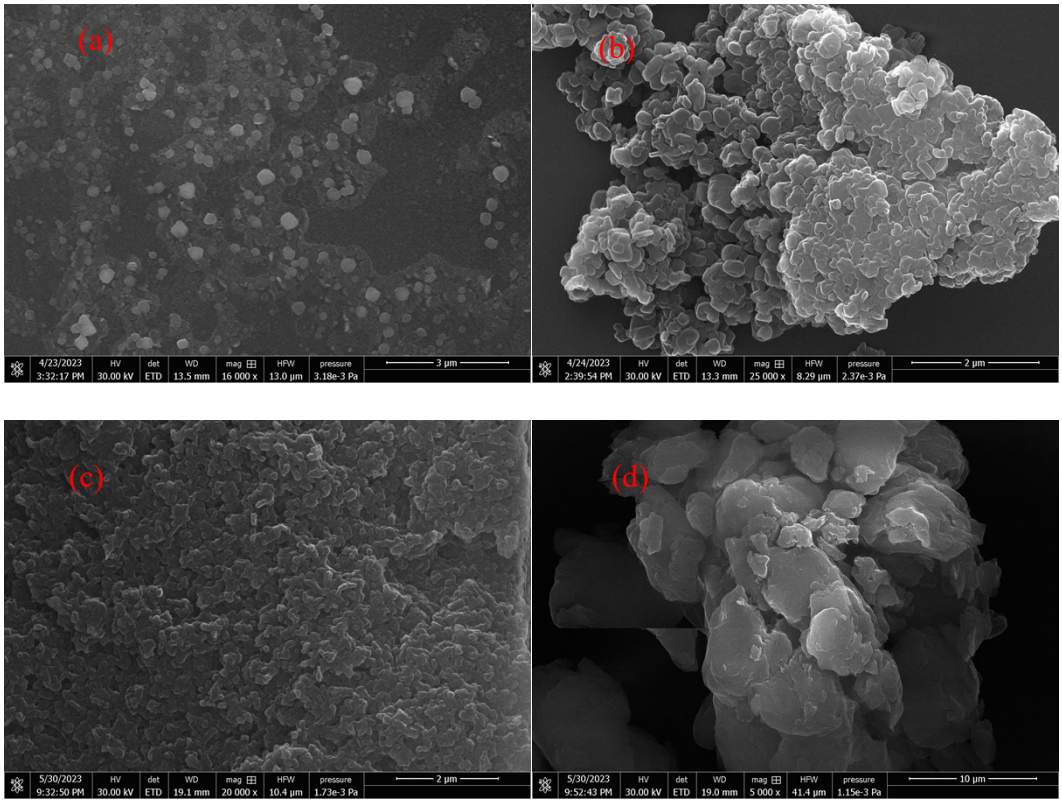

Fig. S7: SEM images of **1**: (a) the precipitates in aqueous solution comprised of particles in a wide range of sizes, and most them with sizes of much less 300 nm, (b, c) the precipitate was dried at 313 and 373 K, and in these case, the aggregated flakes show uniform size, with maximum dimension of ca. 300 nm, (d) the green microcrystals with size of 1–2 μm (ref. Fig. S1) after ground, which look like waxy.

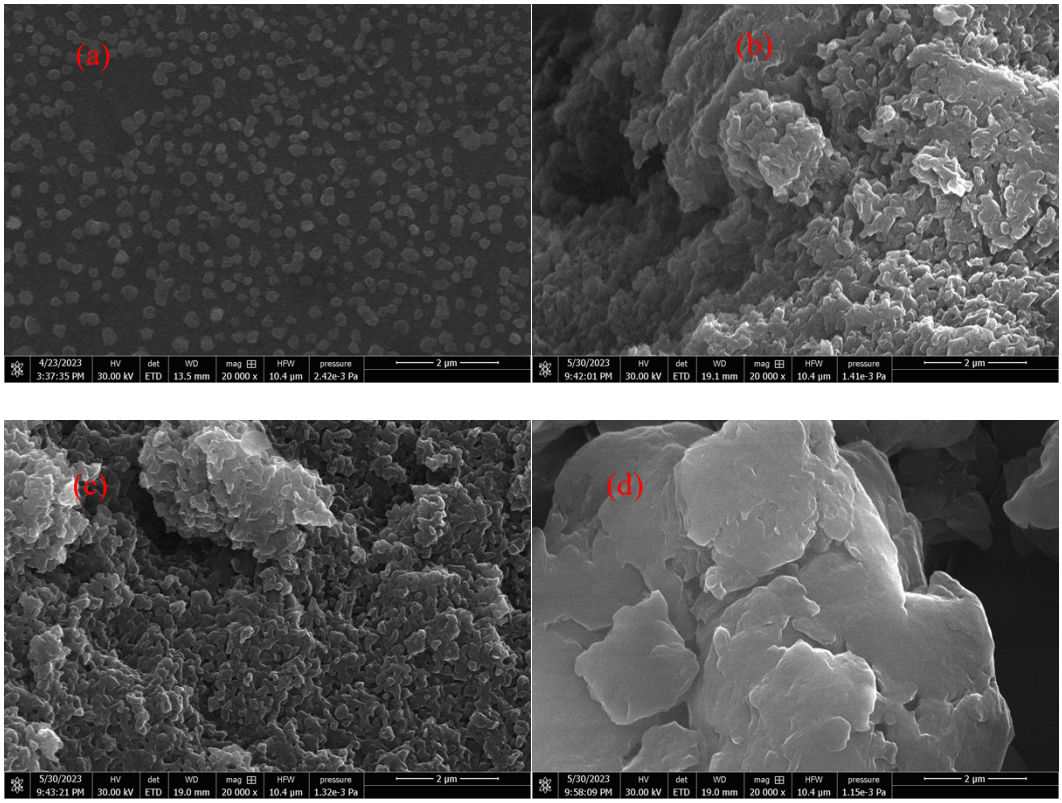

Fig. S8: SEM images of [C_8-4,4'-BiPy][Ni(mnt)$_2$]: (a) the precipitates in aqueous solution comprised of particles in a wide range of sizes, and most them with sizes of much less 300 nm, (b, c) the precipitate was dried at 313 and 373 K, and in these case, the aggregated flakes show uniform size, with maximum dimension of ca. 300 nm, (d) the green microcrystals after ground, which look like waxy.

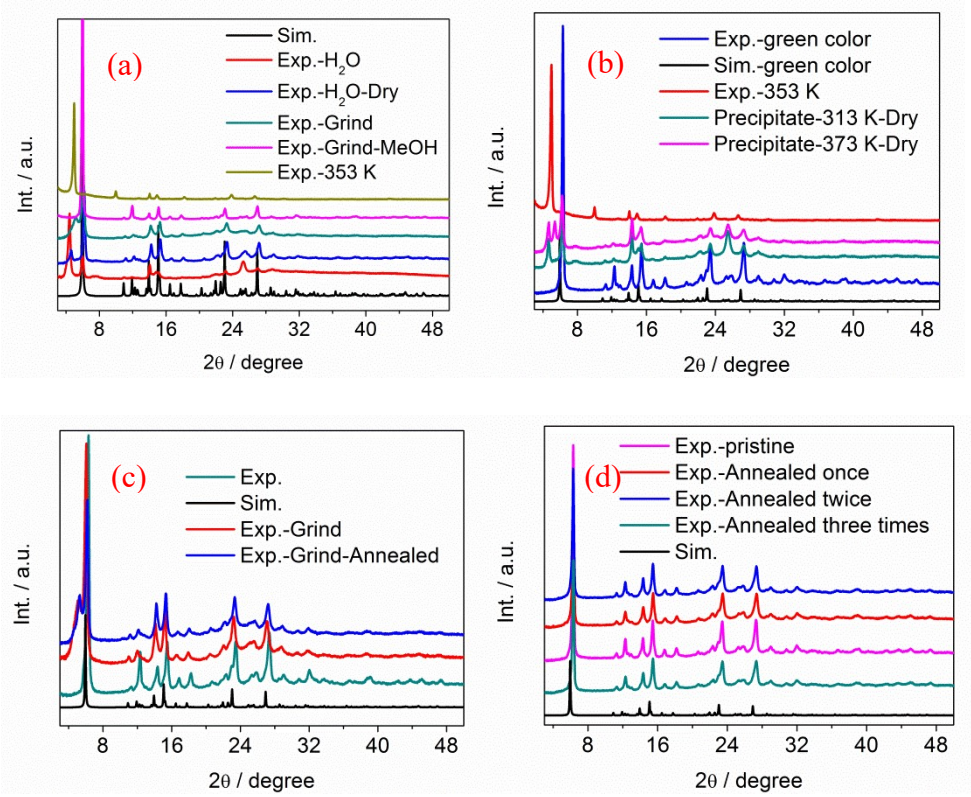

Fig. S9: (a–d) PXRD patterns comparison of the samples of **1** treated at different conditions. In (a) the character strings such as Sim., Exp.-H_2O, Exp.-H_2O-dry, Exp.-Grind, Exp.-Grind-MeOH, Exp.-353 K represent the simulated PXRD pattern from the room temperature single crystal data; precipitates in the aqueous solution; precipitates in the aqueous solution and then dried at 313 K; precipitate dried, ground and then ultrasonically dispersed in MeOH; green microcrystals at 353 K. In (b) the character strings such as Exp.-green color, Sim.-green color, Exp.-353 K, precipitate-313 K-dry and precipitate-373 K-dry, represent the experimental PXRD pattern of green color crystals; the simulated one from the single crystal data at room temperature; green microcrystals at 353 K; precipitates in the aqueous solution and then dried at 313 K; precipitates in the aqueous solution and then dried at 373 K. (c) PXRD patterns of **1**: green crystals, green crystals by grinding, and green crystals by grinding and then by annealing at 373 K. (d) PXRD patterns of **1**: green crystals, green crystals by annealing 1–3 times, simulated PXRD pattern.

It is noted that the samples precipitated in the aqueous solution or by grinding show the character of LTP and HTP mixture of **1**.

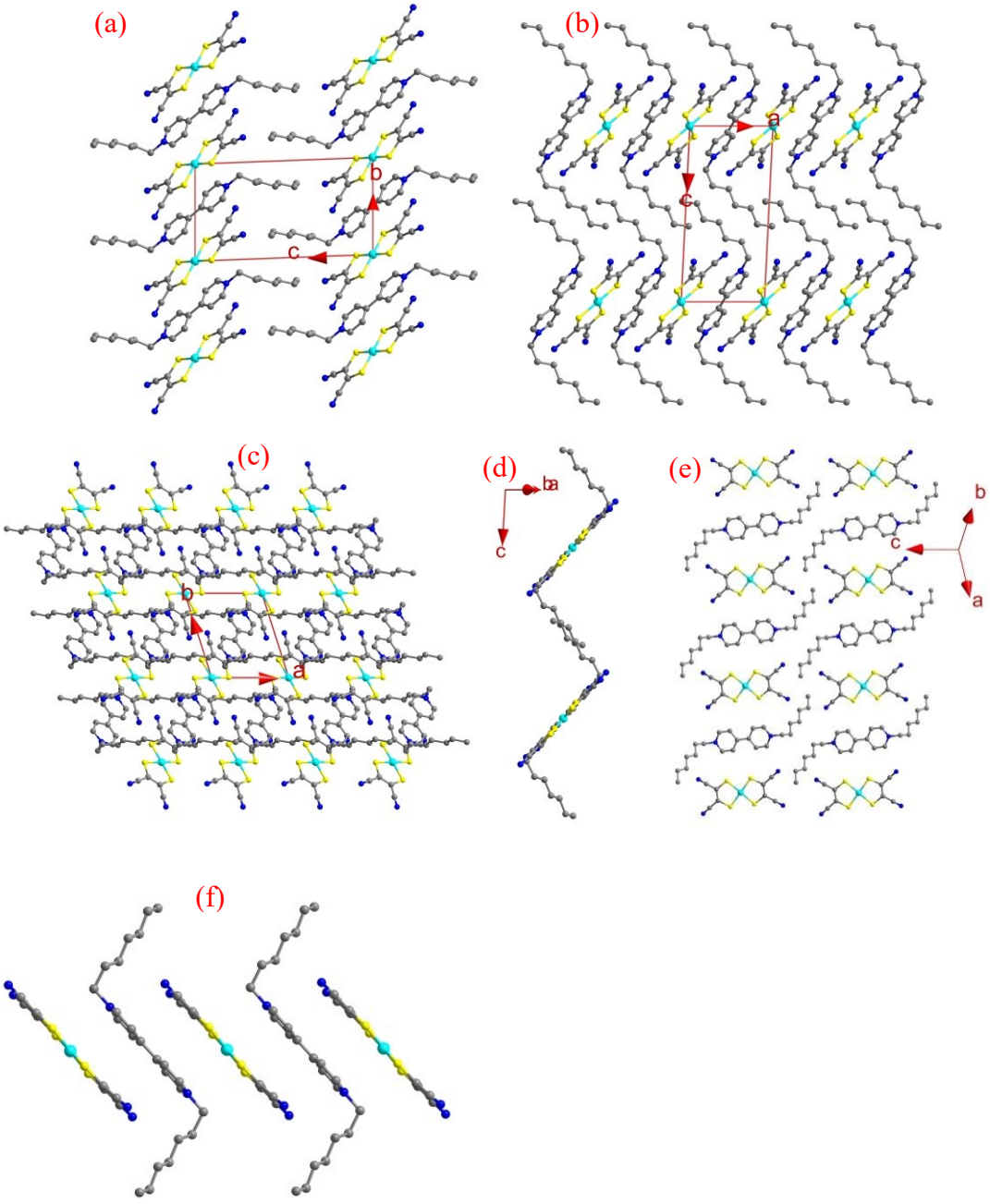

Fig. S10: Packing diagrams viewed along the direction of (a) *a*-axis, (b) *b*-axis, and (c) *c*-axis. The anions and cations form a wrinkle layer, which is parallel to (1 1 0) plane, and (d, e) viewed along [–1 1 0] and [4 4 1] directions, (f) a mixed stack of alternating anion and cation for **1**.

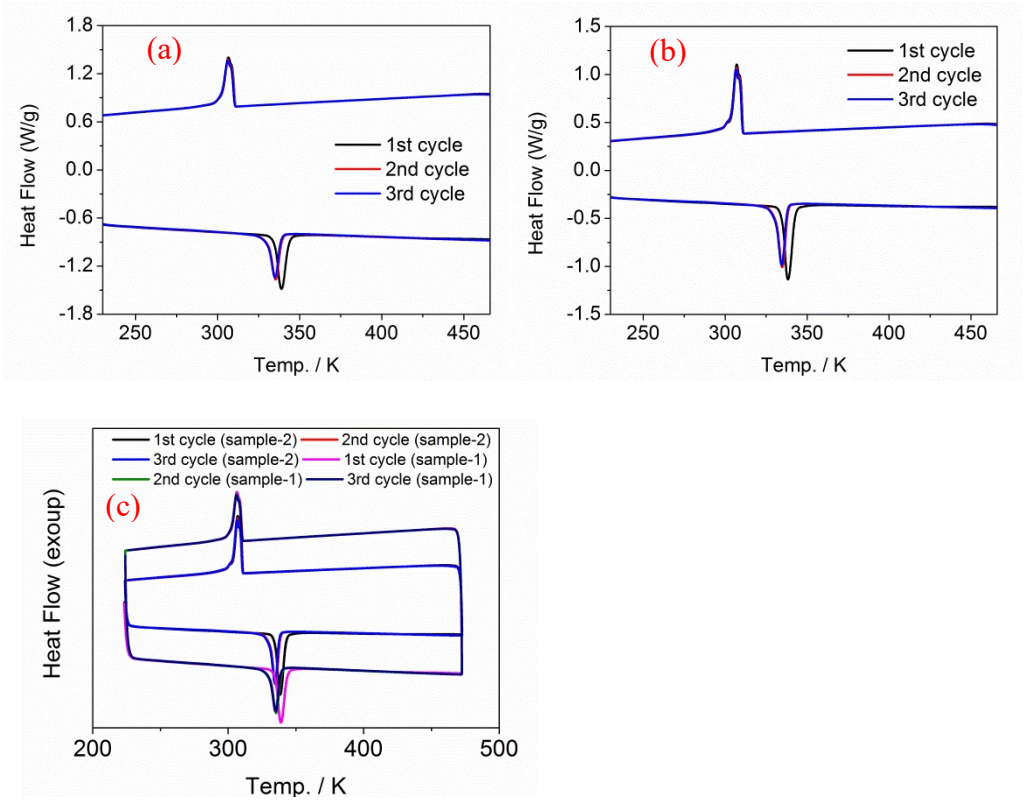

Fig. S11: DSC plots of **1** with three successive heating-cooling cycles (a) sample-1: Nitrogen 50.0 ml/min and (b) sample-2: Nitrogen 100.0 ml/min. (c) DSC plots of comparison for sample-1 and sample-2, indicating that the temperature of phase transition is not affected by the flowing rate of N_2 gas.

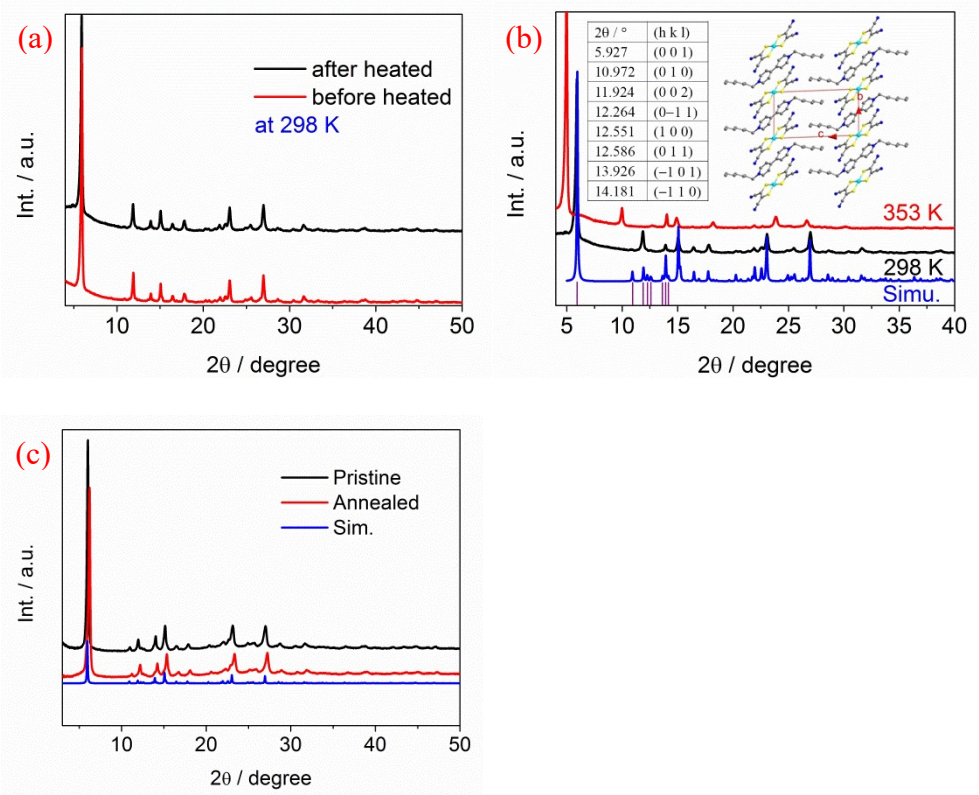

Fig. S12: Variable-temperature PXRD patterns of **1** measured at 298 K for the sample (a) before heated (i.e., the as-synthesized sample) and after heated from 298→323→343→353→363→353→323→298 K, (b) the sample measured at 298 and 353 K together with the simulated pattern using the single crystal structure data at 303 K (inset Table showing the 2θ angles and Miller index of diffractions indicated as well as the packing diagram viewed along *a*-axis). (c) PXRD patterns of **1**, in which the black, red and blue plots represent the patterns of pristine, annealed at 363 K and then cooled down to room tempertaure, and simulated pattern from single crystal structure. The PXRD patterns of pristine sample and the one annealed at 363 K then cooled down to room temperature are almost the same, indicating that the structural phase transition is reversible.

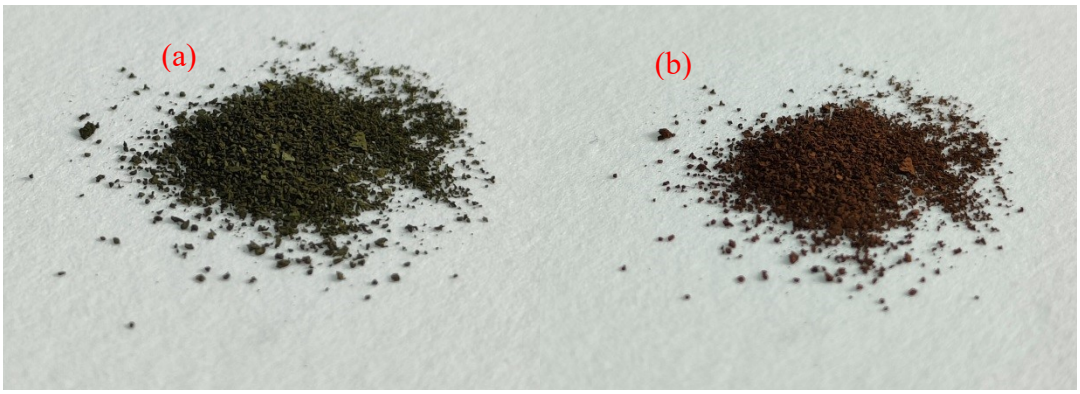

Fig. S13: Photos of microcrystalline sample of $[C_8\text{-}4,4'\text{-BiPy}][Ni(mnt)_2]$ at (a) 303 and (b) 353 K.

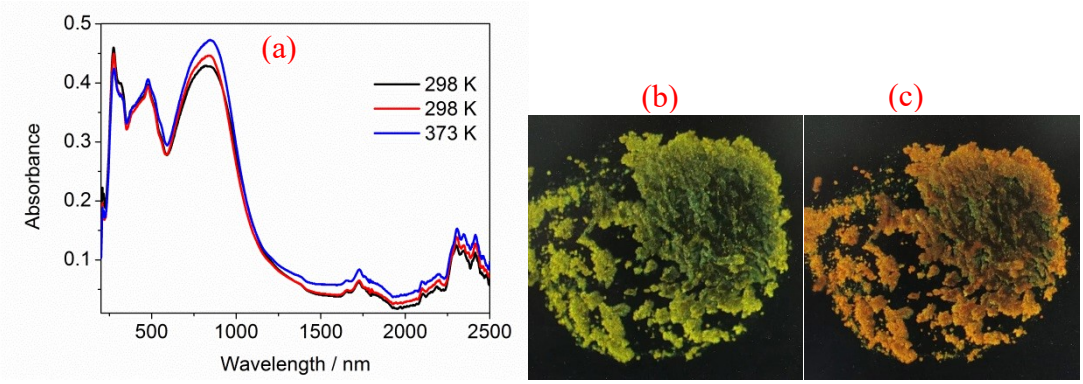

Fig. S14: (a) Solid UV-vis-near-IR spectra at different temperatures, where the black and blue plots represent the spectra of pristine sample at 298 K, 373 K, and the red curve is obtained that the sample was heated to 373 K and then cooled down to 298 K. Photos of microcrystalline sample of **1** at (b) 303 and (c) 353 K.

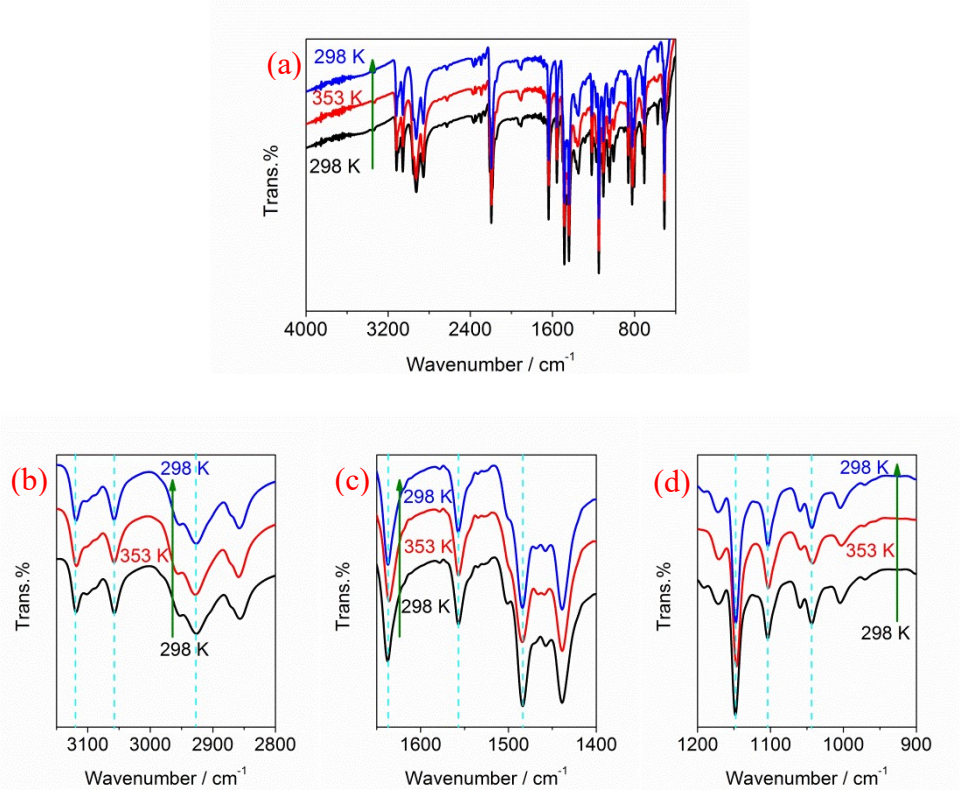

Fig. S15: Variable-temperature IR spectra of **1** in different spectral regions of (a) 4000–400 cm^{-1}, (b) 3150–2800 cm^{-1}, (c) 1650–1400 cm^{-1}, (d) 1200–900 cm^{-1}.

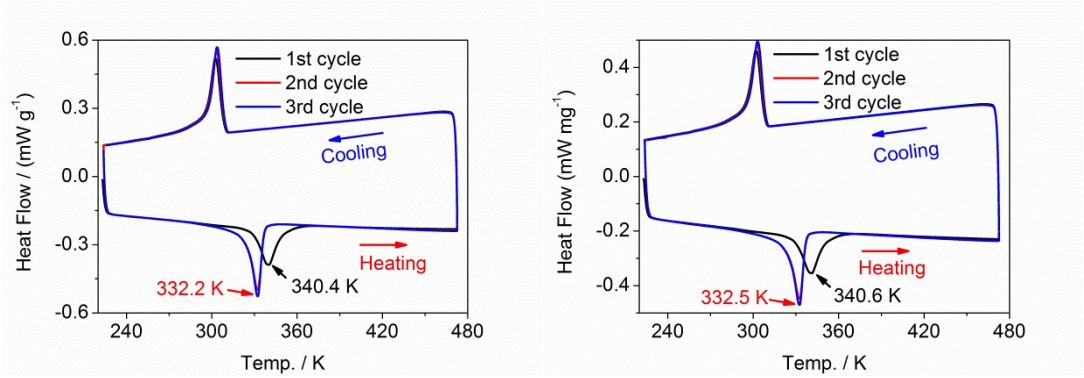

Fig. S16: DSC plots of ground for (a) 3 min, and (b) 5 min, which show one coupling of thermal anomaly with almost the same peak temperatures with the pristine sample of **1**.

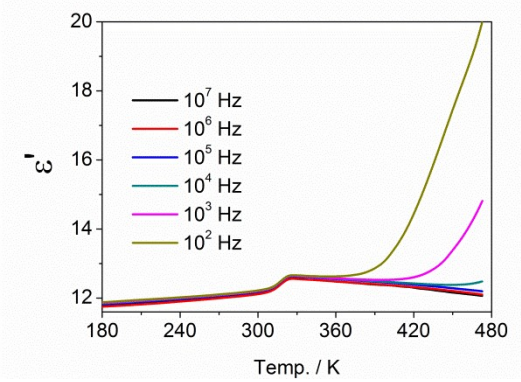

Fig. S17: Temperature dependence of dielectric permittivity of **1** at selected AC frequencies in 180–478 K on cooling.

Table S3: Dielectric constants of some conventional high-κ metal-oxides

Metal oxide	Dielectric constant	*Ref.*
Y_2O_3	12–20	[7]
La_2O_3	21–30	[7]
Sm_2O_3	8.1–14.3	[7]
Eu_2O_3	22.4	[7]
Gd_2O_3	7.4–20	[7]
Dy_2O_3	11–13	[7]
Er_2O_3	9–14	[7]
Yb_2O_3	7–20	[7]
Lu_2O_3	11.6	[7]
Al_2O_3	9	[7, 8]
Ta_2O_5	22	[7, 8]
TiO_2	80	[7, 8]
HfO_2	25	[7, 8]
ZrO_2	25	[7, 8]

References

1. A. Davison, H. R. Holm, *Inorg. Synth.* 1967, **10**, 8–26.
2. H. B. Duan, X. M. Ren, L. J. Shen, W. Q. Jin, Q. J. Meng, Z. F. Tian, S. M. Zhou, *Dalton Trans.* 2011, **40**, 3622–3630.
3. Bruker, *APEX 2*, *SAINT*, *XPREP*, Bruker AXS Inc., Madison, Wisconsin, USA, 2007.
4. Bruker, *SADABS*, Bruker AXS Inc., Madison, Wisconsin, USA, 2001.
5. G. M. Sheldrick, *Acta Crystallogr., Sect. A: Found. Crystallogr.* 2008, **64**, 112−122.
6. C. W. Schläpfer, K. Nakamoto, *Inorg. Chem.* 1975, **14**, 1338−1344.
7. A. Kahraman, S. C. Deevi, E. Yilmaz, *J. Mater. Sci.* 2020, **55**, 7999–8040.
8. J. Robertson, R. M. Wallace, *Mater. Sci. Eng. R* 2015, **88**, 1–41.